Journal of Materials Chemistry A

Accepted Manuscript

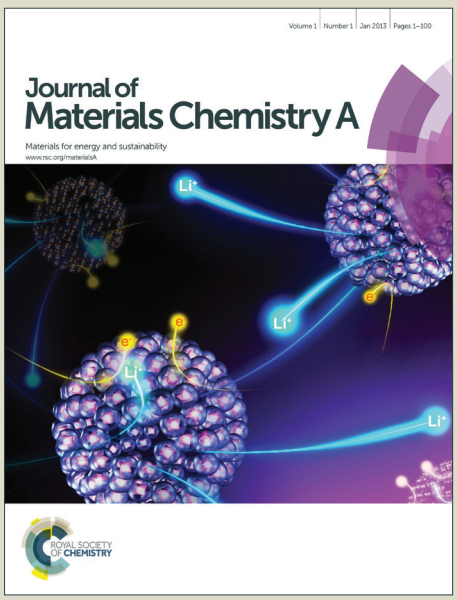

ROYAL SOCIETY OF CHEMISTRY

www.rsc.org/materialsA

Electron Deficient Diketopyrrolopyrrole Dyes for Organic Electronics: Synthesis by Direct Arylation, Optoelectronic Characterization, and Charge Carrier Mobility

Arthur D Hendsbee[1], Jon-Paul Sun[2], Lesley R. Rutledge[1], Ian Hill[2], Gregory C Welch,[1]*

Department of Chemistry[1], Department of Physics[2]
Dalhouise University, 6274 Coburg Road
Halifax, Nova Scotia, Canada B3H 4R2

RECEIVED DATE (automatically inserted by publisher);

ian.hill@dal.ca, gregory.welch@dal.ca

Key Words: Organic Semiconductors, Field-effect transistors, Small molecules, Diketopyrrolopyrrole dyes, Phthalimide, Naphthalimide, Direct Arylation, n-Type mobility

Abstract

Four electron deficient small molecules based on the diketopyrrolopyrrole (DPP) chromophore were synthesized using microwave-assisted direct arylation reactivity. These molecules are based upon an acceptor-donor-acceptor-donor-acceptor (A^1-D-A^2-D-A^1) framework, where DPP is utilized as the central acceptor (A^2) unit. We compared the effect of naphthalimide vs. phthalimide terminal acceptors (A^1), and different DPP (A^2) alkyl groups, on the optical, thermal, electrochemical and electronic properties. A combination of absorption and emission spectroscopy, differential scanning calorimetry, thermal gravimetric analysis, cyclic voltammetry, ultraviolet photoelectron spectroscopy, charge carrier mobility, and DFT calculations were used to characterize the four materials. All compounds were found to have narrow band-gaps, deep HOMO/LUMO levels, and were able to effectively act as electron transport materials.

1. Introduction

The field of organic electronics has seen tremendous growth over the past 25 years.[1,2] Important technologies include light emitting diodes (LED),[3,4] field effect transistors (FET),[5,6] and

photovoltaics (PV).[7,8,] Critical to the advancement of such technologies is the development of new π-conjugated organic materials with tailored properties for specific applications,[9] and thus the role of the synthetic chemist cannot be overstated. One of the major advantages of organic vs. inorganic semiconductors is the breadth of organic building blocks readily available that can be pieced together and systematically tuned to realize desired properties.[10] Over the past several years, the industrial pigment, diketopyrrolopyrrole (DPP),[11] has emerged as one of the most widely used organic building blocks to construct high performance materials for both organic FET[12] and PV[13] applications.

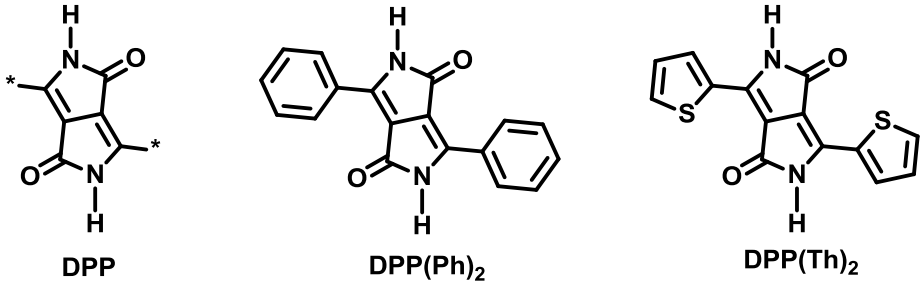

Figure 1. Chemical structure of the diketopyrrolopyrrole (DPP) chromophore and the common phenyl (Ph_2-DPP) and thiophene (Th_2-DPP) based derivatives.

First reported in 1974 by Farnum *et al.*[14], the DPP chromophore (Figure 1) is easily synthesised, has strong visible light absorption, is thermally stable, and can be easily functionalized with aliphatic sides chains on the amide-nitrogen atom, enabling dissolution in common organic solvents.[15,16] Importantly, the presence of two electron-withdrawing amide functional groups render DPP a good acceptor within the context of donor-acceptor (D-A) organic π-conjugated materials.[17,18] The DPP core is commonly substituted in the 3 and 6 positions with phenyl[19] or thienyl[20] substituents ($DPP(Ph)_2$ and $DPP(Th)_2$, respectively, in Figure 1), also, furan[21] and

selenophene[22] substituted DPP have been reported. The smaller, 5-membered heterocyclic rings lead to smaller dihedral angles between the DPP core and the pendant substituent, resulting in greater planarity of the molecular backbone, thus increasing π-delocalization and intermolecular π–π interactions. Additionally, thiophene is a stronger electron donor than phenyl, enhancing intramolecular charge transfer transitions. These effects result in DPP(Th)$_2$ based materials typically exhibiting smaller band gaps and greater charge transport properties than the corresponding DPP(Ph)$_2$ derivatives.[23,24] Both phenyl and thienyl DPP can be synthesized or functionalized with reactive terminal bromine moieties, and thus a wide range of both polymer and small molecule DPP derivatives have been synthesized and used as active components in organic electronic devices.[15] Specifically, DPP based conjugated polymers have be used to fabricate organic PV devices with power conversion efficiencies (PCEs) approaching 10%,[25–27]and organic FET devices with hole mobility above 8 $cm^2\ V^{-1}\ s^{-1}$.[28]

While initially less studied, DPP based small molecules have emerged as some of the most promising materials for use in solution-processed small molecule organic PV devices.[29–31] Pioneering work by Nguyen and co-workers back in 2008 demonstrated the utility of DPP based oligothiophenes as donor materials in fullerene-based (bulk-heterojunction) BHJ solar cells, and achieved PCEs over 3%.[16,32,33] Subsequently, in 2009 the same group showed that PCEs could be improved to 4.4% using benzofuran end-capping units (DPP(ThBzFu)$_2$) in place of oligothiophenes,[34] a record PCE that stood until 2012. These small molecules possessed several advantages to related conjugated polymers, including higher purity, simplified synthesis, and the ability for absolute structure determination via single crystal X-ray diffraction.[29,35,36] With respect to the latter, precise structure determination has enabled accurate structure-property-function

correlations.[37–39] As such, this work paved the way for the emergence of small molecule based organic PVs, which now compare to their polymer-fullerene counterparts in highest recorded PCE.[40–42]

Less widely studied, are electron transporting (n-type) DPP small molecules which have the potential to be used in place of fullerene derivatives. Significant improvements in the performance of non-fullerene based organic solar cells have been realized over the past year with PCEs reaching 4% and 5%, using small molecule[43] and polymer[44] based acceptors, respectively. Replacing fullerenes with D-A type materials can lead to greater photon harvesting through increased absorption of the acceptor, higher open circuit voltages through better BHJ energy level alignment, and potential increased chemical stability and lower material production costs. We refer the reader to several recent reviews for details.[44–50] There are several reports of BHJ solar cells comprising DPP based small molecules as electron acceptors[51,52] and poly-3-hexylthiophene (P3HT) as an electron donor, with a best PCE of 2.05% being acheived.[53]

Based on these results, we became interested in the design and synthesis of electron deficient DPP-based small molecules that have appropriate energy levels and absorption profiles that could be used as n-type materials in optoelectronic devices. In line with the work of Chen *et al*[51], we envisioned that flanking the DPP core with electron deficient end-capping units bearing aliphatic sides chains would lead to materials with narrow band gaps, deep frontier molecular orbital energy levels, and the ability to efficiently transport electrons. Herein we report on the optimized synthesis, materials characterization, and electron mobility of a series of DPP based small molecules incorporating electron-deficient phthalimide and naphthalimide end-capping units.

2. Design, Computational Analysis, and Synthesis

2.1 Materials Design

Highlighted in Figure 2 is the design strategy we utilized to generate electron deficient narrow band gap π-conjugated organic small molecules. These materials are based upon a π-DPP-π framework. As previously discussed, the $DPP(Th)_2$ core ensures deep HOMO/LUMO levels and strong visible light absorption. We utilized terminal aryl-imide groups to further increase the electron affinity of the small molecule and thus further lower the HOMO/LUMO energies. Aryl imides are also know to promote self-assembly via strong π–π interactions,[54] and many derivatives are commercially available at low cost, an important aspect for potential large scale production.[55,56] Importantly, this framework incorporates alkyl side chains both perpendicular and parallel to the π-conjugated backbone, which can both be readily tuned. Such orthogonal positioning of alkyl side chains has proven successful in yielding uniform and highly ordered thin-films of 'donor' small molecules from solution.[57,58] For this study we compare the impact of phthalimide vs. naphthalimide end groups (**1** vs. **2**), and octyl vs. 2-ethylhexyl vs. 2-hexyldecyl (**2** vs. **3** vs. **4**) aliphatic side chains on key optical, thermal, and electronic properties relevant to organic electronics.

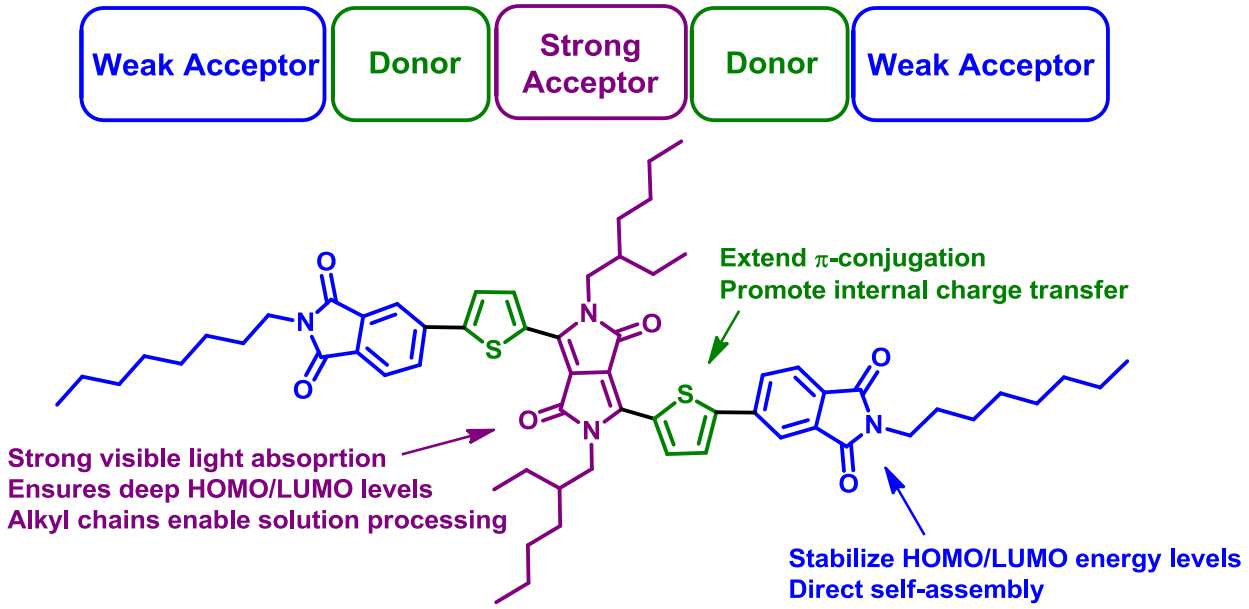

Figure 2. Design strategy to achieve electron deficient narrow band gap small molecules.

2.2 Computational Analysis

To support our hypothesis that the naphthalimide and phthalimide end-capping units should increase the electron affinity of the DPP small molecules, we utilized gas-phase density functional theory (DFT) to analyze truncated structures (full details provided in the SI), and compared to the well-studied small molecule DPP(ThBzFu)$_2$ (3,6-bis[5-(benzofuran-2-yl)-thiophen-2-yl]-2,5-bis(2-ethylhexyl)pyrrolo[3,4-c]pyrrole-1,4-dione)[34]. Molecular geometries for the two core structures featuring naphthalimide and phthalimide end-capping units and DPP(ThBzFu)$_2$ were optimized at the B3LYP 6-31G(d,p) level of theory (Figure 3). For the naphthalimide and phthalimide structures, the thiophene ring and DPP core are nearly coplanar. Not surprisingly, the larger naphthalimide end-cap is significantly twisted (ca. 45°) out of the DPP(Th)$_2$ plane (Figure 3a). The smaller phthalimide end cap is only ~20° distorted from planarity with the core DPP(Th)$_2$ (Figure 3b). Similar observations have been made for related compounds with vinyl-

benzo[c]1,2,5-thiadiazole cores,[54] although the steric issues are more pronounced in the present case due to aryl-aryl interactions rather than aryl-vinyl interactions. The deviation from planarity at the ends of the molecule is in contrast to DPP(ThBzFu)$_2$ which adpots a near-planar conformation in the gas-phase between the thiophene and benzofuran rings (torsion angle = ca. 0.4°, Figure 3c). The thiophene rings and the DPP core are slighly out of plane, in opposite directions, for DPP(ThBzFu)$_2$, resulting in a slight bowing of the π-conugated backone and a reduction of dipole moment. The larger dipole moments for the napthalimide and phthalimide structures might have consequences on solid-state molecular assembly.[59] The calculated highest occupied molecular orbitals (HOMOs) and lowest unoccupied molecular orbitals (LUMOs) for the naphthalimide and phthalimide structures were found to be much deeper than that of DPP(ThBzFu)$_2$, supporting the notion that electron-withdrawing imide groups render the π-conjugated backbone electron deficient. In addition, the HOMOs and LUMOs are more localized and delocalized, respectively, for these structures when compared to DPP(ThBzFu)$_2$, again highlighting the electron-withdrawing nature of the imide end-capping units.

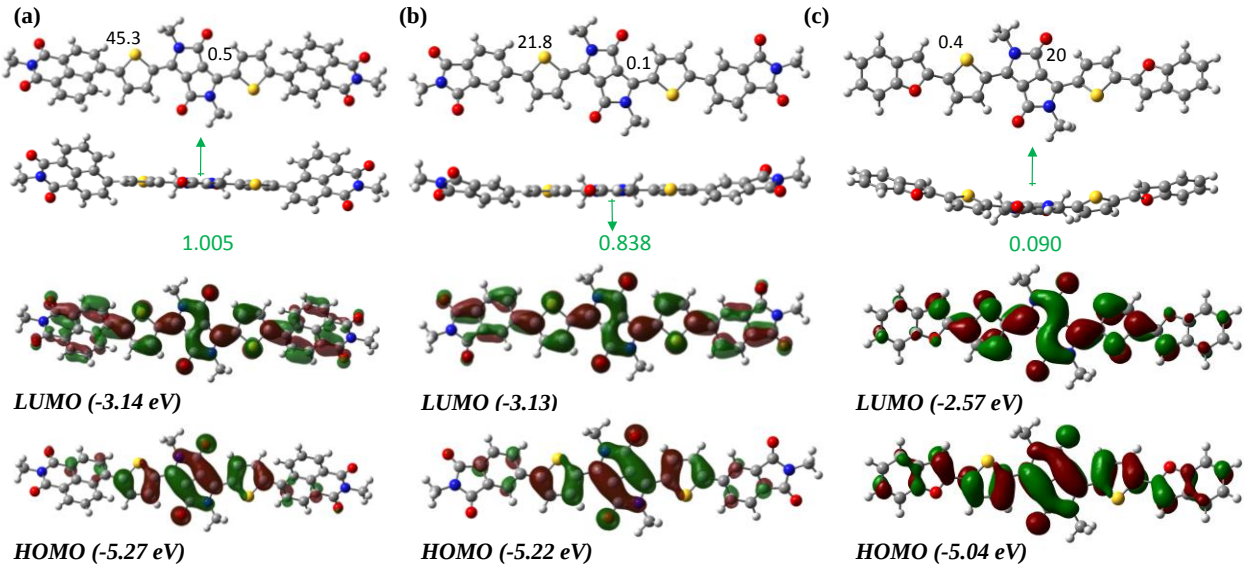

Figure 3. Results from B3LYP/6-31G(d,p) calculations comparing the DPP(Th)$_2$ core with naphthalimide (**1**, a) phthalimide (**2,3,4** structure; b) and benzofuran (DPP(ThBzFu)$_2$); c) end-capping units. Angle between adjacent ring planes (degrees, °) shown in black text (top structures). Dipole moment vectors and magnitudes (Debyes, D) are shown in green. HOMO/LUMO molecular orbital diagrams are shown below with calculated energy values.

2.3 Synthesis

The core DPP(Th)$_2$ (2,5-dihydro-1,4-dioxo-3,6-dithienylpyrrolo[3,4-c]-pyrrole) was first prepared by using well known synthetic methods.[14,60] The resulting red pigment is insoluble in practically all solvents due to strong intermolecular hydrogen bonding between adjacent DPP units with the N-H as the donor and the ketone oxygen as an acceptor.[61–63] To disrupt these strong intermolecular forces and enable dissolution in organic solvents, alkyl groups may be attached to the amide functionality using N-alkylation reactions. Traditional methods utilize conventional heating and require purification via column chromatography. We first modified the reaction step and found that the N-alkylation of DPP(Th)$_2$ can be facilitated using microwave irradiation, yielding product in under 60 minutes. Second, the workup procedure was modified for this work and it was found that recrystallization from hot ethanol produces pure alkyl-DPP(Th)$_2$, removing the need for column chromatography and organic solvents which are commonly employed to purify alkyl-DPP(Th)$_2$ compounds. See Supporting Information for full details. The resulting alkyl-DPP(Th)$_2$ dyes are deep-red in color and soluble in common processing solvents, which allows for further reactivity.

The four target small molecules were synthesized from the alkyl-DPP(Th)$_2$ and appropriate brominated end-capping units via direct arylation (DA) (Figure 4).[64,65] This method directly couples aryl-H and aryl-Br reactants allowing for C-C bond formation without the use of toxic tin reagents, phosphorus based ligands, or cumbersome boronic acids that are commonly seen in other C-C bond forming reactions, increasing atom economy and decreasing environmental impact.

While traditional DA reactions are carried out using conventional heating over several hours, we found that the reactions could be easily accelerated using microwave heating (17 minutes at 170°C). The final product dyes were a rich blue color and were purified via flash chromatography. Microwave heating was successful in producing pure samples of compounds **1**, **2**, **3**, and **4** with isolated yields of 31%, 62%, 62%, and 63%, respectively. Compounds **1**-**4** were structurally characterized by ^{1}H and ^{13}C NMR spectroscopy and mass spectroscopy (See supporting information for full details on synthesis and spectroscopic characterization). All compounds were determined to be soluble in common organic solvents including chloroform, toluene, and chlorobenzene.

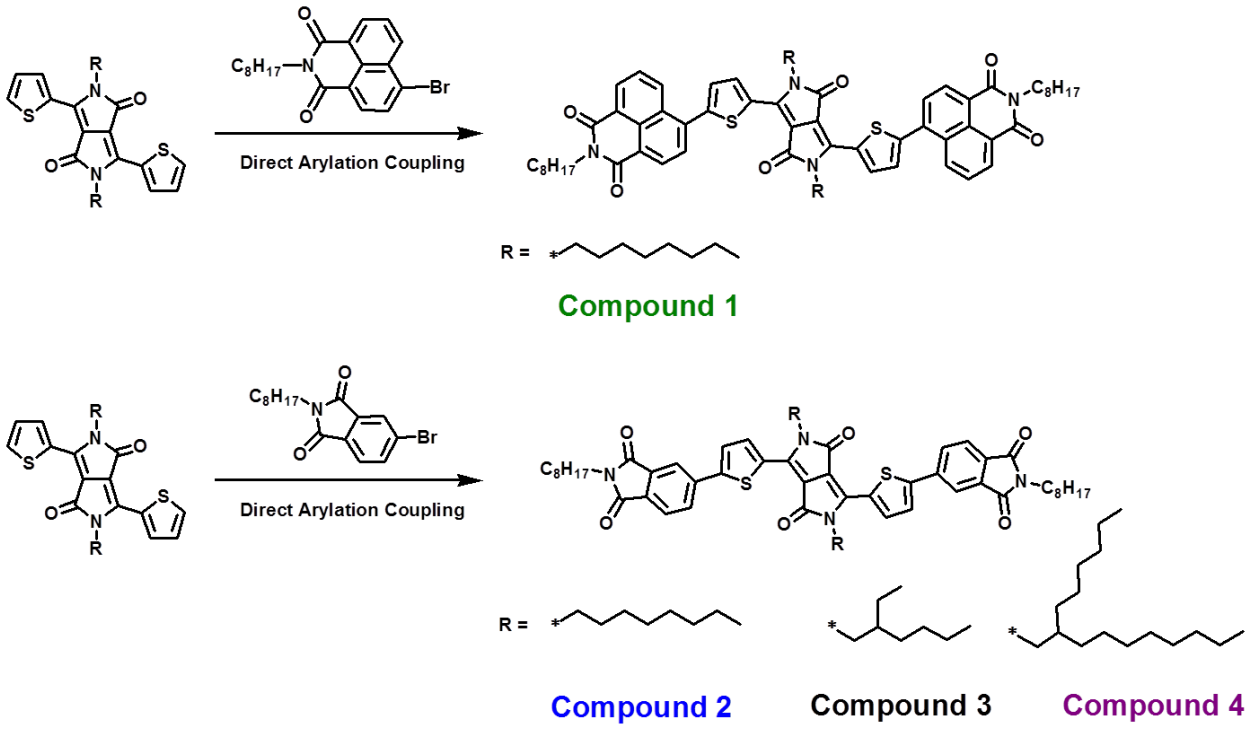

Figure 4. General synthetic route towards compounds **1**-**4**. Direct arylation conditions: $Pd(OAc)_2$, Pivalic Acid, K_2CO_3, DMA, Microwave irradiation 170°C, 17 minutes.

3. Optical Absorption and Emission Spectroscopy

The ability of compounds **1-4** to absorb and emit light was examined using UV-visible and photoluminescence spectroscopy. Results are summarized in Table 1. Figure 5 (a and b) shows the individual absorption profiles of all compounds in $CHCl_3$ solution. All compounds have similar absorption profiles with strong low energy bands at ~600 nm and slightly weaker high energy bands at ~400 nm. These profiles are common for DPP based small molecules, with the low energy and high energy bands attributed to D-A charge transfer transitions and localized π–π transitions, respectively (see Supporting Information for confirmation via theoretical calculations). Compound **1,** featuring naphthalimide end-capping units displayed a broad absorbance spectrum which showed minimal fine structure, with absorption max (λ_{max}) blue shifted compared to compounds **2-4**, thus implying that the large naphthalene unit may be distorting the molecular backbone from planarity in solution, which could reduce the effective conjugation length of the molecule. Compounds **2-4**, which feature phthalimide end-capping units, all display two distinct low energy absorption peaks which we attribute to a more rigid structure in solution, due to less steric strain between the C_6 and C_5 rings. This was confirmed by variable temperature UV-visible absorption experiments, where heating solutions of **2** or **4** in chlorobenzene resulted in loss of fine structure due to increased rotation about the aryl C-C bonds (see Supporting Information). Interestingly, compound **3** with 2-ethylhexyl side chains on the DPP core has a sharp onset of absorption at ~745 nm, whereas compounds **1** and **2** with *n*-octyl DPP side chains and compound **4** with 2-hexyldecyl DPP side chains, exhibit broad, tailing absorption onsets in $CHCl_3$ solution. The origin of the broad absorption onsets for compounds **1**, **2** and **4** is not entirely known at this point.

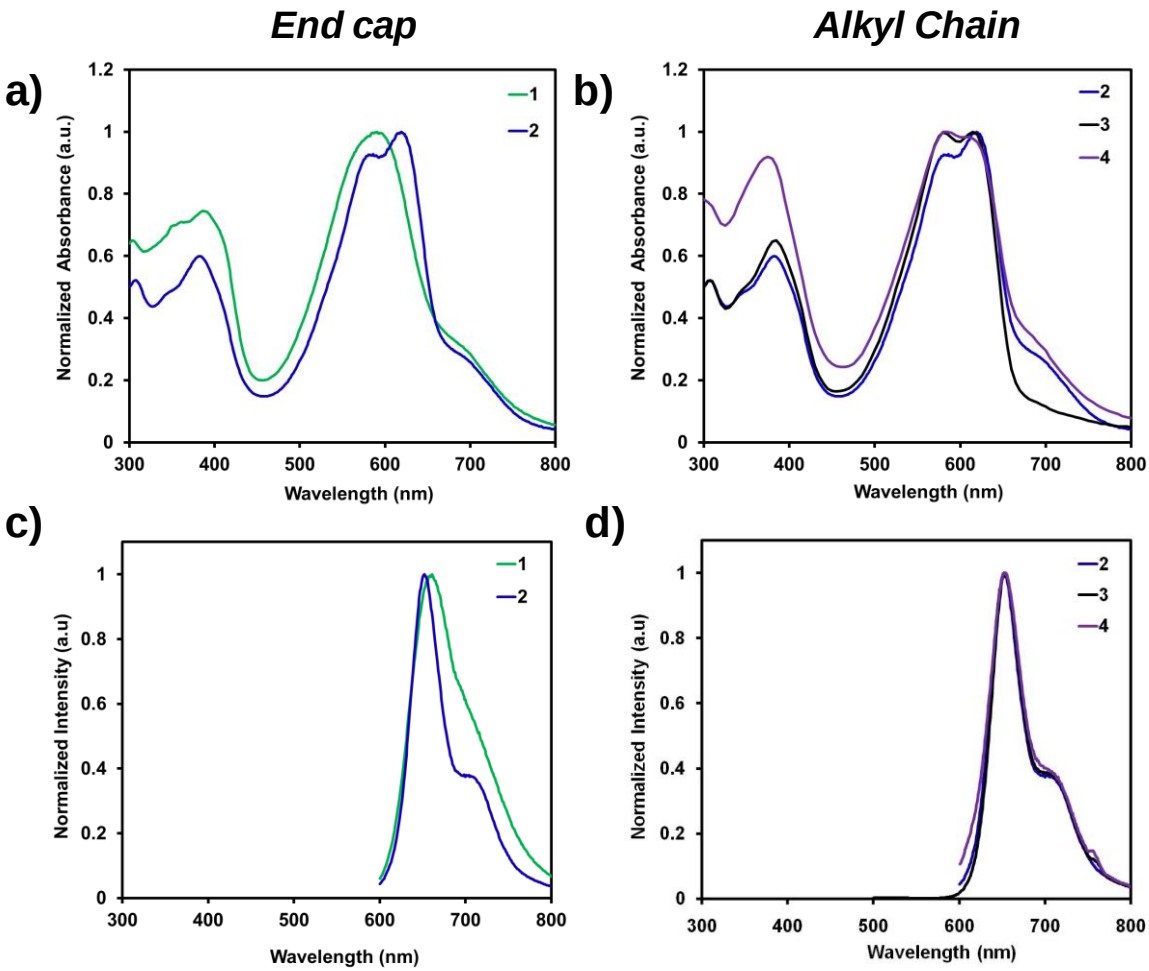

Figure 5. a-b) Normalized solution UV-Visible spectroscopy for compounds **1**-**4** in $CHCl_3$ solution at room temperature. c-d) Normalized solution fluorescence spectroscopy for compounds **1**-**4** in $CHCl_3$ at room temperature.

The photoluminescence spectra of compounds **1**-**4** are shown in Figure 5 (c-d), with full details in Table 1. All compounds exhibit a similar profile with a strong emission band at ~650 nm and a small shoulder at ~750 nm, except that of compound **1**, which has a broad and feature-less profile, similar to the absorption spectrum. Compound **1** also exhibits the largest Stokes shift (ca. 72 nm). These observations are consistent with **1** adopting a non-planar structure in solution.

Thin-films of compounds **1-4** were spin-coated onto glass substrates and their absorption profiles were obtained before and after thermal annealing. The absorption profile of the thin films is red-shifted compared to the solution spectra (Figure 6). This effect has been noted in many dyes and is ascribed to an increase in probability of low energy transitions due to long range ordering of aromatic molecules in the solid state.[66,67] Comparing compounds **1** and **2** (Figure 6a), compound **2** has a broader and slightly better defined low energy absorption band, again a likely result of the phthalimide end-cap leading to a more rigid π-conjugated backbone. Quite surprisingly, increasing the topology (the amount and shape of the space occupied by the alkyl chains) and length of the DPP alkyl side chain (Figure 6b) resulted in an increase in the fine structure and intensity of the low energy absorption bands. Comparing **2** and **3** (*n*-octyl vs. 2-ethylhexyl DPP side chains), a sharpening of the low energy band is observed to give two peaks, a maximum at ~615 nm and a shoulder at ~655 nm. Increase in both the length and topology of the of DPP side chain to 2-hexyldecyl (compound **4**), leads to a very sharp absorption profile with two distinct low energy bands at ~630 nm and ~690 nm. Our thought is that the larger/longer 2-hexyldecyl side chains are likely crystallizing with each other in the solid state, bringing the π-conjugated backbones of molecules closer together and locking in place a favorable 'face-on' orientation. Similar observations have been made in the literature.[68,69] Compound **3** featuring slightly smaller 2-ethylhexyl side chains displays similar, but less defined, vibronic structure in its solid state absorption spectra compared to **4**. Compounds **1** and **2** featuring the *n*-octyl side chains showed the least vibronic structure in both the solution and solid state absorption profiles among all compounds. It should be noted that the use of 2-hexyldecyl DPP cores has typically resulted in the construction of the best performing materials for organic PV applications.[70]

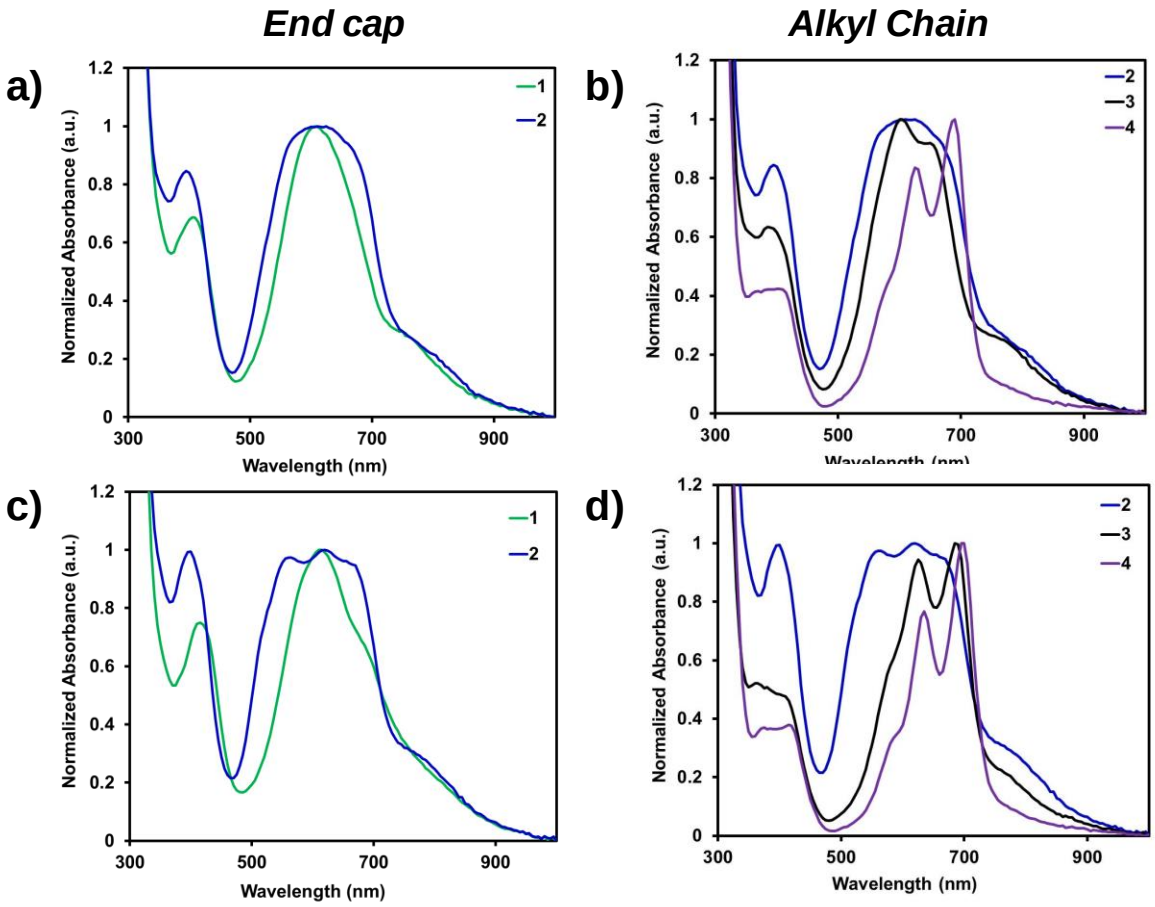

Figure 6. Normalized UV-Visible spectra thin-films of compounds **1**-**4**. a-b) as-cast from 1% $CHCl_3$ solutions, and c-d) thermally annealed at 100°C for 10 minutes in air**.**

DPP small molecules are known to undergo molecular rearrangement in the solid-state upon thermal[34,39] or solvent annealing.[71] Thermally annealing the thin-films at 100°C for ten minutes resulted in a red-shift in λ_m for compounds **1**, **3**, and **4** and a very small blue-shift for compound **2**. The onset of absorption (λ_o) is red shifted for **1** and **4** upon annealing and is slightly blue shifted for compounds **2** and **3.** For compounds **2**-**4**, an increase in the fine structure of the low energy bands were observed, with the band at ~700 nm dominating all absorption profiles. For **1**, minimal

change is observed in the absorption profile upon thermal annealing, a likely result of the bulky naphthalimide end groups preventing the formation of strong intermolecular π–π interactions.

4. Thermal Properties

Differential Scanning Calorimitrey (DSC) was used to probe the thermal transitions of compounds **1**-**4**. Compound **1** exhibits a weak melting transition at ~189 °C and no crystallization transition is observed. In contrast, compound **2**, incorporating the smaller phthalimide end-cap undergoes a melt in the solid phase at a much higher temperature of ~261 °C, and a corresponding crystallization transition at ~245 °C is observed (Figure 7a). These data are in line with **1** having a more disordered structure in the solid-state. A decrease in melting transition is observed upon increasing the size and branching of the alkyl chain on DPP from ~260 °C for **2** with octyl groups, to ~183 °C for **3** with 2-ethylhexyl groups, and to ~139 °C for **4** with 2-hexyldecyl groups (Figure 6b). Similar trends have been reported on in the literature,[19,57] and are attributed to a change in the ratio of π-π interactions to alkyl-alkyl interactions. As the alkyl chain length increases and the conjugated part of the molecule stays the same size, alkyl-alkyl interactions may begin to dominate the process of self-assembly instead of the π-conjugated part of the molecule.[70] It is interesting to note that compound **3** with 2-ethylhexyl groups shows no crystallization transition, while compounds **2** and **4** with smaller and larger alkyl side chains, respectively, exhibit distinct crystallization transitions (Figure 7). Overall, based on these observations, it is clear that large naphthalene based end-groups and bulky alkyl side chains decreases the melting points of the compounds. Thermogravimetric analysis (TGA) was used to measure the decomposition temperature of the four DPP compounds. For compounds **1**-**4**, the decomposition temperatures are all relatively similar. All compounds exhibited excellent structural integrity in air, with decomposition temperatures above 350°C (Figure 7c and d, Table 1).

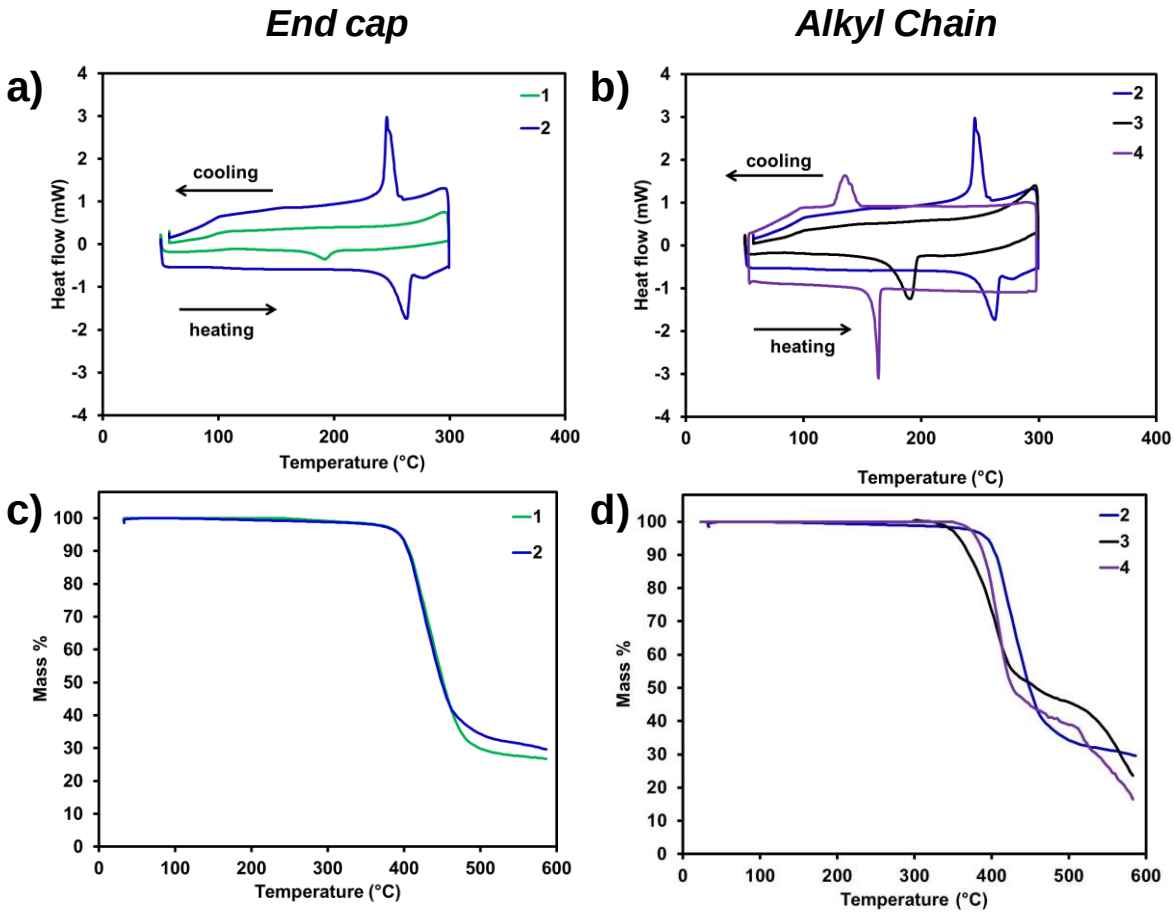

Figure 7. a-b) Differential Scanning Calorimetry for compounds **1-4.** Compounds were heated from 50°C to 300°C for three cycles under air. c-d) Thermogravimetric analysis for compounds **1**-**4**. Compounds were heated to 600°C at 15k/min under a N_2 atmosphere**.**

Table 1: Selected Optical and Thermal properties for compounds **1**-**4**

	Solution			***Thin Film***					***Thermal Properties***		
	$\lambda_m{}^a$	$\lambda_o{}^a$	$\lambda_{em}{}^a$	$\lambda_m{}^b$	$\lambda_o{}^b$	E_g	$\lambda_m{}^d$	$\lambda_o{}^d$	T_m	T_c	T_d
1	589	764	661	605	760	1.66	610	770	189	-	396
2	618	766	652	625	760	1.66	620	750	261	243	403
3	615	745	654	600	740	1.70	685	735	183	-	361
4	590	765	654	690	730	1.73	695	735	139	163	369

λ_m = wavelength of maximum absorbance (nm)
λ_o = wavelength of absorbance onset (nm)
λ_{em} = wavelength of maximum emittance, excited at λ_m for each compound (nm)
E_g = optical band gap (1260/ λ_o)

[a] $CHCl_3$ solution
[b] Thin film, spin cast from 1% wt/v in $CHCl_3$
[d] Thin film, spin cast from 1% wt/v in $CHCl_3$, annealed at 100 °C for 10 minutes.
T_m = melting temperature (°C)
T_c = crystallization temperature (°C)
T_d = decomposition temperature (°C)

5. Frontier Molecualr Orbitals Determinaiton.

5.1. Cyclic Voltammetry

Cyclic voltammetry in CH_2Cl_2 solution, was used to determine the electrochemical properites for compound **1-4**, as shown in Figure 8. All compounds exhbited two distinct reversible oxidation and reduction peaks. The highest occupied molecular orbital (HOMO) and lowest unoccupied molecular orbital (LUMO) energy levels of all four compounds were estimated from the onset of oxidation and reduction, respectively; data are presented in Table 2. Compounds **2**-**4** have deep HOMO levels from ~ -5.1 to -5.2 eV, and relatively low lying LUMO levels from ~ -3.4 to -3.6 eV. These values are in the expected range for DPP based small molecules, and are comparable to related DPP compounds utilizing electron-withdrawing fluorophenyl end caps,[51,64] but are lower in energy that those utilizing thiophene based end-caps.[16,72] The fact that all compounds have similar oxidation and reduction potentials in solution, indicates that the electronic structure is not strongly affected by the addition of two extra phenyl rings (**1** vs **2**) or the nature of solubilizing end group (**2** vs **3** vs **4**) at the molecular level.

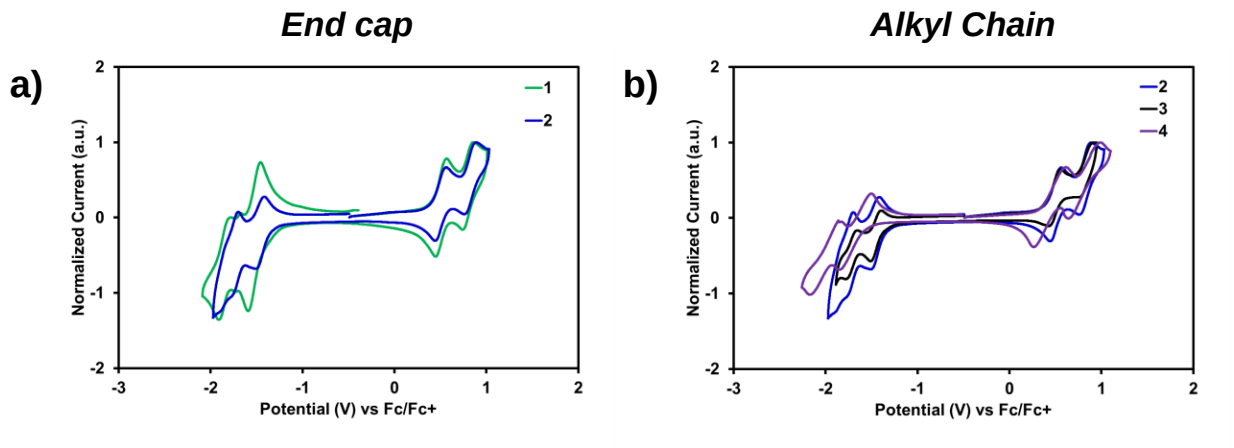

Figure 8. Cyclic voltammograms for compounds **1**-**4** obtained in CH_2Cl_2 solution under an N_2 atmosphere using a sweep rate = 100 mV/s.

Table 2: Frontier molecular orbital determination results for compounds **1**-**4**

	UPS/Optical			*CV*			*DFT*	
	HOMO	**LUMO** [a]	**Eg**	**HOMO** [b]	**LUMO** [c]	**Eg**	**HOMO** [d]	**LUMO** [d]
1	-5.4	-3.7	1.66	-5.20	-3.58	1.62	-5.27	-3.14
2	-5.2	-3.5	1.66	-5.13	-3.54	1.59	-5.22	-3.13
3	-5.2	-3.5	1.70	-5.11	-3.54	1.57	-5.22	-3.13
4	-5.3	-3.6	1.73	-5.18	-3.39	1.79	-5.22	-3.13
DPP(ThBzFu)$_2$ [e]	-5.0	-3.7	1.70	-5.20[f]	-3.40[f]	n/a	-5.04	-2.57

[a]Determined using the thin-film onset of absoption (optical band gap) and UPS determined HOMO value
[b] Determined from the onset of oxidation in CH_2Cl_2 solution (referenced to ferrocene)
[3] Determined from the onset of reduction in CH_2Cl_2 solution (referenced to ferrocene)
[d] From DFT calculations at the B3LYP/6-31(d,p) level of theory
[e] UPS values independently determined by our research group for direct comparions to **1-4**.
[f] Values taken from literature.[34]

5.2. Ultraviolet Photoelectron Spectroscopy

Ultraviolet photoelectron spectroscopy was used as a second method of determining the HOMO of compounds **1-4**. This method can be considered more relevant to organic PV, since measurements are carried out on thin-films. Results are summarized in Table 2 with plots shown

in Figure 9. All compounds show similar HOMOs, with compound **1** exhibiting a slightly deeper value (-5.4 eV) and compounds **2** and **3** having slightly higher values (-5.2 eV). Compound **4** sits in the middle at -5.3 eV. In the solid state, compound **1** has a deeper HOMO than **2**, whereas in solution they have similar oxidation onsets. DFT calculations revealed that compound **1** is predicted to exhibit significant twisting between the DPP core and the naphthalimide end-caps in the gas phase, and as a result of the decreased planarity, the HOMO is calculated to be lower than that of **2**, following a similar trend to the UPS values. Therefore, this distortion from planarity likely exists in the solid state, deepening the HOMO energy levels. The effect of alkyl chain substitution between **2**, **3** and **4** is subtle, and differences could be due to solid-state packing configurations affecting the polarization response to the photo-ionized molecule. However, these small differences in HOMO values are on the order of experimental uncertainty of the measurement. For comparison to the well-studied DPP(ThBzFu)$_2$ small molecule [34,73] we measured the HOMO of DPP(ThBzFu)$_2$ via UPS to be -5.0 eV, 0.2 eV higher than compound **3**. This difference can be explained by the greater π-electron deficiency of phthalimide compared to benzofuran, thus highlighting the electron withdrawing effect of the phthalimide end-capping unit.

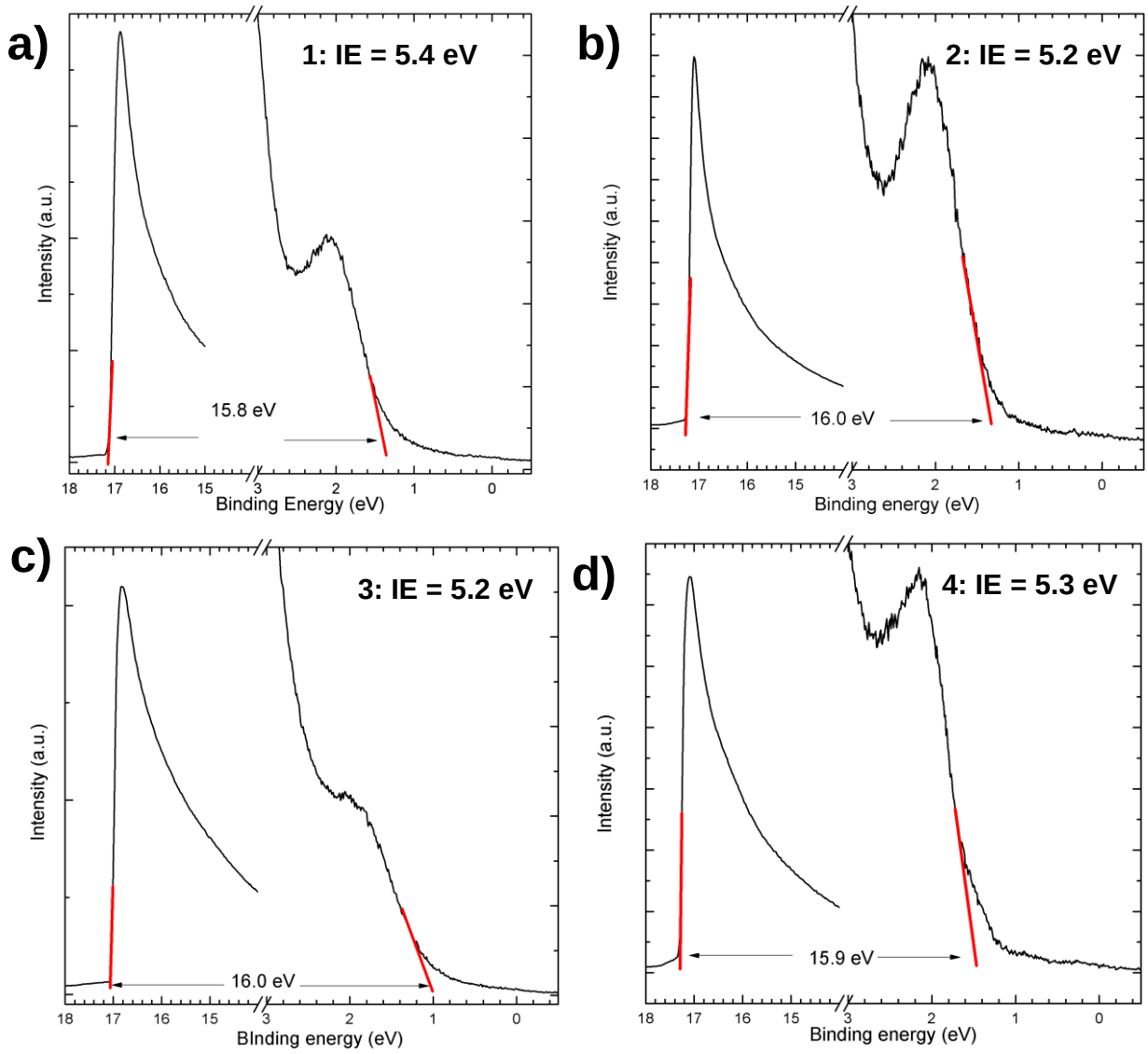

Figure 9. Ultraviolet Photoelectron Spectroscopy for compounds **A) 1**, **B) 2**, **C) 3**, **D) 4**. Red lines indicate the energies used to calculate the ionization energy (IE) for each compound.

6. Charge Carrier Mobility

To evaluate the ability of compound **1-4** to transport electrons and be suitable n-type materials for use in optoelectronic devices, we measured the charge carrier mobility of each by fabricating n-channel bottom-gate top-contact transistors, using aluminum (Al) electrodes (see SI for complete details). All compounds are found to transport electrons in this configuration (Table 3). Compounds **2** and **4** show the highest electron mobility, with values of 1.2 x 10^{-3} and 1.9 x 10^{-3}

cm^2/Vs, respectively. Compound **3** with 2-ethylhexyl side chains exhibited a two orders of magnitude lower mobility, with a value of 3.4×10^{-5} cm^2/Vs. Compound **1** with naphthalimide end capping units shows the lowest mobility with a value of 1.1×10^{-6} cm^2/Vs. The lower value of **1** compared to the others is likely a result of the non-planar π-conjugated backbone (*vide supra*) preventing the formation of strong intermolecular π–π interactions required for rapid charge transport. While it is difficult to comment on the absolute solid-state packing of these materials without single-crystal structures, the lower mobility of **3** compared to **2** and **4**, is in-line with the absence of strong melting or crystallization peaks in the DSC plots, indicating that the 2-ethylhexyl groups might be disrupting the formation of ordered nanostructures under these conditions, and/or be orientated face on with the substrate. In all cases, the n-type charge carrier mobilites are slightly lower than that reported for PCBM ($\sim 10^{-2}$ cm^2/Vs).[74] The n-type mobility of compounds **1-4** was also compared to the standard DPP(ThBzFu)$_2$. To the best of our knowledge, the n-type mobility of DPP(ThBzFu)$_2$ has not been reported. In our device configuration with a thermally evaporated active layer, a transistor electron mobility (μ_e) of 1.2×10^{-4} ($cm^2V^{-1}s^{-1}$) was found for DPP(ThBzFu)$_2$. In comparison, compounds **2** and **4** had higher n-type mobility by nearly one order of magnitude. Interestingly, DPP(ThBzFu)$_2$, bearing 2-ethylhexyl chains on the DPP core exhibited higher mobility than compound **3** which also contains the same alkyl chains on the DPP core. There is no clear reason for this, however the fact that compound **3** bears alkyl chains on the end-capping units and DPP(ThBzFu)$_2$ does not could play a role in the crystal packing, and therefore the charge transport ability. Nonetheless, the ability of compounds **1-4** to retain (compounds **1**, **3**) and possibly improve upon (compounds **2** and **4**) the electron transporting ability of DPP(TBzFu)$_2$ validates our design strategy of end capping the DPP chromophore with electron

deficient units as an effective way to generate materials with suitable properties for use as acceptors in organic solar cell devices.

Table 3: n-Channel field effect transisitor data for compounds **1-4** and DPP(ThBzFu)$_2$

Compound	μ_e ($cm^2V^{-1}s^{-1}$)	V_T (V)	I_{on}/I_{off}
1	1.1×10^{-6}	40	10^1
2	1.2×10^{-3}	15	10^3
3	3.4×10^{-5}	25	10^2
4	1.9×10^{-3}	11	10^3
DPP(ThBzFu)$_2$	1.2×10^{-4}	21	10^1

7. Conclusion

We have reported on the design and synthesis of four narrow band gap, electron deficient, small molecules based upon the diketopyrrolopyrrole (DPP) dye. The incorporation of imide based end-capping units on the DPP core served to increase the electron affinity of the π-conjugated backbone and stabilized the HOMO and LUMO energy levels, relative to the well-studied compound DPP(ThBzFu)$_2$. Importantly, each compound was synthesized in high yields using microwave assisted direct arylation reactivity, thus avoiding the use of coupling functional groups and prolonged reaction times. All compounds were found to have narrow optical band gaps ranging from 1.66 to 1.73 eV and high thermal stabilities. Compounds bearing naphthalimide end-capping units exhibited significant twisting of the π-conjugated backbone. The large deviation from planarity for the naphthalimide DPP small molecule (**1**) resulted in a large observed Stokes shift, broad and featureless absorption profiles, and low melting transitions, as such a non-planar structure can inhibit the formation of strong intermolecular π–π interactions. Phthalimide based

molecules (**2**-**4**) were found to adopt a more planar ground state structure and had better defined absorption spectra and sharper melting transitions. All compounds were found to transport electrons, with phthalimide based compounds exhibiting the highest mobilites. These findings suggest that the simple and cost-effective phthalimide building block can be used to construct narrow-band gap, electron transporting materials, and should be given more attention in future molecular design.

8. Acknowledgments

GCW and IGH acknowledgment the Natural Science and Engineering Council of Canada Discovery programs for funding this work. JPS thanks Killam Trusts, NSERC CGS, and Dalhousie Research in Advanced Materials, Energy, and Sustainability (DREAMS) program for a financial support. We would also like to thank the reviewers of this manuscript who provide very insightful suggestions.

9. References

1. L. Dou, J. You, Z. Hong, Z. Xu, G. Li, R. A. Street, and Y. Yang, *Adv. Mater.*, 2013, **25**, 6642–6671.
2. Huanli Dong, Xiaolong Fu, Jie Liu, Zongrui Wang, and Wenping Hu, *Adv. Mater.*, 2013.
3. A. C. Grimsdale, K. Leok Chan, R. E. Martin, P. G. Jokisz, and A. B. Holmes, *Chem. Rev.*, 2009, **109**, 897–1091.
4. H. Zheng, Y. Zheng, N. Liu, N. Ai, Q. Wang, S. Wu, J. Zhou, D. Hu, S. Yu, S. Han, W. Xu, C. Luo, Y. Meng, Z. Jiang, Y. Chen, D. Li, F. Huang, J. Wang, J. Peng, and Y. Cao, *Nat Commun*, 2013, **4**.
5. C. Wang, H. Dong, W. Hu, Y. Liu, and D. Zhu, *Chem. Rev.*, 2011, **112**, 2208–2267.
6. J. Terao, A. Wadahama, A. Matono, T. Tada, S. Watanabe, S. Seki, T. Fujihara, and Y. Tsuji, *Nat Commun*, 2013, **4**, 1691.
7. Y.-W. Su, S.-C. Lan, and K.-H. Wei, *Mater. Today*, 2012, **15**, 554–562.
8. Y. Sun, G. C. Welch, W. L. Leong, C. J. Takacs, G. C. Bazan, and A. J. Heeger, *Nat Mater*, 2012, **11**, 44–48.
9. P. M. Beaujuge and J. M. J. Fréchet, *J. Am. Chem. Soc.*, 2011, **133**, 20009–20029.
10. J. Roncali, *Macromol. Rapid Commun.*, 2007, **28**, 1761–1775.
11. M. J. Robb, S.-Y. Ku, F. G. Brunetti, and C. J. Hawker, *J. Polym. Sci. Part Polym. Chem.*, 2013, **51**, 1263–1271.
12. C. B. Nielsen, M. Turbiez, and I. McCulloch, *Adv. Mater.*, 2013, **25**, 1859–1880.
13. S. Qu and H. Tian, *Chem. Commun.*, 2012, **48**, 3039–3051.
14. D. G. Farnum, G. Mehta, G. G. I. Moore, and F. P. Siegal, *Tetrahedron Lett.*, 1974, **15**, 2549–2552.
15. D. Chandran and K.-S. Lee, *Macromol. Res.*, 2013, **21**, 272–283.
16. A. B. Tamayo, B. Walker, and T.-Q. Nguyen*, *J. Phys. Chem. C*, 2008, **112**, 11545–11551.
17. Y.-J. Cheng, S.-H. Yang, and C.-S. Hsu, *Chem. Rev.*, 2009, **109**, 5868–5923.

18. D. Gendron and M. Leclerc, *Energy Environ. Sci.*, 2011, **4**, 1225–1237.
19. C. Kim, J. Liu, J. Lin, A. B. Tamayo, B. Walker, G. Wu, and T.-Q. Nguyen, *Chem. Mater.*, 2012, **24**, 1699–1709.
20. J. C. Bijleveld, A. P. Zoombelt, S. G. J. Mathijssen, M. M. Wienk, M. Turbiez, D. M. de Leeuw, and R. A. J. Janssen, *J. Am. Chem. Soc.*, 2009, **131**, 16616–16617.
21. C. H. Woo, P. M. Beaujuge, T. W. Holcombe, O. P. Lee, and J. M. J. Fréchet, *J. Am. Chem. Soc.*, 2010, **132**, 15547–15549.
22. A. J. Kronemeijer, E. Gili, M. Shahid, J. Rivnay, A. Salleo, M. Heeney, and H. Sirringhaus, *Adv. Mater.*, 2012, **24**, 1558–1565.
23. S. Stas, J.-Y. Balandier, V. Lemaur, O. Fenwick, G. Tregnago, F. Quist, F. Cacialli, J. Cornil, and Y. H. Geerts, *Dyes Pigments*, 2013, **97**, 198–208.
24. H. Bürckstümmer, A. Weissenstein, D. Bialas, and F. Würthner, *J. Org. Chem.*, 2011, **76**, 2426–2432.
25. L. Dou, J. You, J. Yang, C.-C. Chen, Y. He, S. Murase, T. Moriarty, K. Emery, G. Li, and Y. Yang, *Nat Photon*, 2012, **6**, 180–185.
26. K. H. Hendriks, G. H. L. Heintges, V. S. Gevaerts, M. M. Wienk, and R. A. J. Janssen, *Angew. Chem. Int. Ed.*, 2013, **52**, 8341–8344.
27. W. Li, A. Furlan, K. H. Hendriks, M. M. Wienk, and R. A. J. Janssen, *J. Am. Chem. Soc.*, 2013, **135**, 5529–5532.
28. H. Chen, Y. Guo, G. Yu, Y. Zhao, J. Zhang, D. Gao, H. Liu, and Y. Liu, *Adv. Mater.*, 2012, **24**, 4618–4622.
29. Q. Huang and H. Li, *Chin. Sci. Bull.*, 2013, **58**, 2677–2685.
30. A. Mishra and P. Bäuerle, *Angew. Chem. Int. Ed.*, 2012, **51**, 2020–2067.
31. B. Walker, C. Kim, and T.-Q. Nguyen, *Chem. Mater.*, 2010, **23**, 470–482.
32. A. B. Tamayo, M. Tantiwiwat, B. Walker, and T.-Q. Nguyen, *J. Phys. Chem. C*, 2008, **112**, 15543–15552.
33. A. B. Tamayo, X.-D. Dang, B. Walker, J. Seo, T. Kent, and T.-Q. Nguyen, *Appl. Phys. Lett.*, 2009, **94**, -.
34. B. Walker, A. B. Tamayo, X.-D. Dang, P. Zalar, J. H. Seo, A. Garcia, M. Tantiwiwat, and T.-Q. Nguyen, *Adv. Funct. Mater.*, 2009, **19**, 3063–3069.
35. Y. Li, Q. Guo, Z. Li, J. Pei, and W. Tian, *Energy Env. Sci*, 2010, **3**, 1427–1436.
36. P. Q. Li Zaifang, *Chin J Org Chem*, 2012, **32**, 834–851.
37. J. Liu, Y. Zhang, H. Phan, A. Sharenko, P. Moonsin, B. Walker, V. Promarak, and T.-Q. Nguyen, *Adv. Mater.*, 2013, **25**, 3645–3650.
38. J. Liu, B. Walker, A. Tamayo, Y. Zhang, and T.-Q. Nguyen, *Adv. Funct. Mater.*, 2013, **23**, 47–56.
39. W. Shin, T. Yasuda, G. Watanabe, Y. S. Yang, and C. Adachi, *Chem. Mater.*, 2013, **25**, 2549–2556.
40. Y. Chen, X. Wan, and G. Long, *Acc. Chem. Res.*, 2013, **46**, 2645–2655.
41. J. E. Coughlin, Z. B. Henson, G. C. Welch, and G. C. Bazan, *Acc. Chem. Res.*, 2013.
42. V. Gupta, A. K. K. Kyaw, D. H. Wang, S. Chand, G. C. Bazan, and A. J. Heeger, *Sci Rep*, 2013, **3**.
43. X. Zhang, Z. Lu, L. Ye, C. Zhan, J. Hou, S. Zhang, B. Jiang, Y. Zhao, J. Huang, S. Zhang, Y. Liu, Q. Shi, Y. Liu, and J. Yao, *Adv. Mater.*, 2013, **25**, 5791–5797.
44. A. Facchetti, *Mater. Today*, 2013, **16**, 123–132.
45. T. Liu and A. Troisi, *Adv. Mater.*, 2013, **25**, 1038–1041.
46. E. Kozma and M. Catellani, *Dyes Pigments*, 2013, **98**, 160–179.
47. P. Hudhomme, *EPJ Photovolt*, 2013, **4**, 40401.
48. C. L. Chochos, N. Tagmatarchis, and V. G. Gregoriou, *RSC Adv*, 2013, **3**, 7160–7181.
49. P. Sonar, J. P. Fong Lim, and K. L. Chan, *Energy Env. Sci*, 2011, **4**, 1558–1574.
50. J. E. Anthony, *Chem. Mater.*, 2010, **23**, 583–590.
51. P. Sonar, G.-M. Ng, T. T. Lin, A. Dodabalapur, and Z.-K. Chen, *J Mater Chem*, 2010, **20**, 3626–3636.
52. Y. Lin, P. Cheng, Y. Li, and X. Zhan, *Chem Commun*, 2012, **48**, 4773–4775.
53. Y. Lin, Y. Li, and X. Zhan, *Adv. Energy Mater.*, 2013, **3**, 724–728.

54. J. T. Bloking, X. Han, A. T. Higgs, J. P. Kastrop, L. Pandey, J. E. Norton, C. Risko, C. E. Chen, J.-L. Brédas, M. D. McGehee, and A. Sellinger, *Chem. Mater.*, 2011, **23**, 5484–5490.
55. T. P. Osedach, T. L. Andrew, and V. Bulovic, *Energy Env. Sci*, 2013, **6**, 711–718.
56. D. J. Burke and D. J. Lipomi, *Energy Env. Sci*, 2013, **6**, 2053–2066.
57. Z. B. Henson, G. C. Welch, T. van der Poll, and G. C. Bazan, *J. Am. Chem. Soc.*, 2012, **134**, 3766–3779.
58. G. C. Welch, L. A. Perez, C. V. Hoven, Y. Zhang, X.-D. Dang, A. Sharenko, M. F. Toney, E. J. Kramer, T.-Q. Nguyen, and G. C. Bazan, *J Mater Chem*, 2011, **21**, 12700–12709.
59. C. J. Takacs, Y. Sun, G. C. Welch, L. A. Perez, X. Liu, W. Wen, G. C. Bazan, and A. J. Heeger, *J. Am. Chem. Soc.*, 2012, **134**, 16597–16606.
60. S. Loser, C. J. Bruns, H. Miyauchi, R. P. Ortiz, A. Facchetti, S. I. Stupp, and T. J. Marks, *J. Am. Chem. Soc.*, 2011, **133**, 8142–8145.
61. J. Mizuguchi and G. Rihs, *Berichte Bunsenges. Für Phys. Chem.*, 1992, **96**, 597–606.
62. J. Mizuguchi, *J. Phys. Chem. A*, 2000, **104**, 1817–1821.
63. O. P. Lee, A. T. Yiu, P. M. Beaujuge, C. H. Woo, T. W. Holcombe, J. E. Millstone, J. D. Douglas, M. S. Chen, and J. M. J. Fréchet, *Adv. Mater.*, 2011, **23**, 5359–5363.
64. S.-Y. Liu, M.-M. Shi, J.-C. Huang, Z.-N. Jin, X.-L. Hu, J.-Y. Pan, H.-Y. Li, A. K.-Y. Jen, and H.-Z. Chen, *J. Mater. Chem. A*, 2013, **1**, 2795–2805.
65. L. G. Mercier and M. Leclerc, *Acc. Chem. Res.*, 2013, **46**, 1597–1605.
66. P. Sonar, E. L. Williams, S. P. Singh, S. Manzhos, and A. Dodabalapur, *Phys Chem Chem Phys*, 2013, **15**, 17064–17069.
67. T. M. Pappenfus, K. B. Schliep, A. Dissanayake, T. Ludden, B. Nieto-Ortega, J. T. López Navarrete, M. C. Ruiz Delgado, and J. Casado, *J. Chem. Educ.*, 2012, **89**, 1461–1465.
68. Y. Li, P. Sonar, L. Murphy, and W. Hong, *Energy Env. Sci*, 2013, **6**, 1684–1710.
69. C. Piliego, T. W. Holcombe, J. D. Douglas, C. H. Woo, P. M. Beaujuge, and J. M. J. Fréchet, *J. Am. Chem. Soc.*, 2010, **132**, 7595–7597.
70. T. Lei, J.-Y. Wang, and J. Pei, *Chem. Mater.*, 2013.
71. A. Viterisi, N. Fernandez-Montcada, V. K. Challuri, F. Gispert-Guirado, E. Martin, E. C. Escudero, and E. J. Palomares, *J. Mater. Chem. A*, 2013.
72. B. Walker, X. Han, C. Kim, A. Sellinger, and T.-Q. Nguyen, *ACS Appl. Mater. Interfaces*, 2011, **4**, 244–250.
73. Z. Li, X. Zhang, Y. Zhang, C. F. Woellner, M. Kuik, J. Liu, T.-Q. Nguyen, and G. Lu, *J. Phys. Chem. C*, 2013, **117**, 6730–6740.
74. T. D. Anthopoulos, D. M. de Leeuw, E. Cantatore, S. Setayesh, E. J. Meijer, C. Tanase, J. C. Hummelen, and P. W. M. Blom, *Appl. Phys. Lett.*, 2004, **85**, 4205–4207.

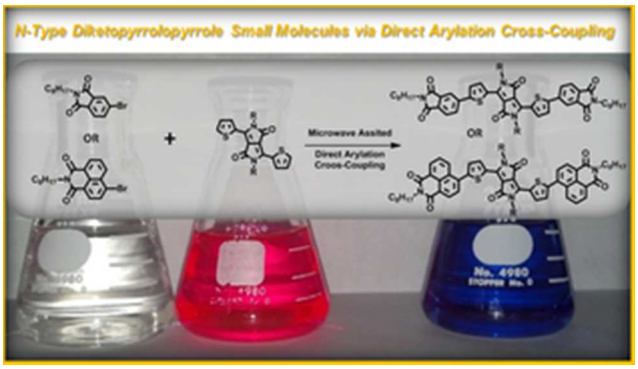

26x15mm (300 x 300 DPI)